ESC European Society of Cardiology

European Heart Journal - Imaging Methods and Practice (2024) **2**, 1–9
https://doi.org/10.1093/ehjimp/qyae007

ORIGINAL ARTICLE

Four-dimensional analysis of aortic root motion in normal population using retrospective multiphase computed tomography

Xun Yuan [1,2,†], Xiaoxin Kan[3,4,†], Jianpeng Li[5], Yang Yan[5], Saeed Mirsadraee [2,6], Tarun Mittal[2,6], Andrew Shah[7], Debbie Saunders[7], Xiao Yun Xu[4], and Christoph A. Nienaber [1,2,*]

[1]Cardiology and Aortic Centre, Royal Brompton & Harefield Hospitals, Guy's and St Thomas' NHS Foundation Trust, Sydney Street, London SW3 6NP, UK
[2]National Heart and Lung Institute, School of Medicine, Imperial College London, Exhibition Road, London SW7 2BX, UK
[3]Center for Vascular Surgery and Wound Care, Jinshan Hospital, Fudan University, Shanghai, China
[4]Department of Chemical Engineering, Imperial College London, London, UK
[5]Department of Cardiovascular Surgery, First Affiliated Hospital of Xi'an Jiaotong University, Xi'an, China
[6]Department of Radiology, Royal Brompton & Harefield Hospitals, Guy's and St Thomas' NHS Foundation Trust, London, UK
[7]Department of Radiology, East and North Hertfordshire NHS Foundation Trust, Middlesex, UK

Received 30 October 2023; accepted after revision 30 January 2024; online publish-ahead-of-print 5 February 2024

Abstract

Aims

Aortic root motion is suspected to contribute to proximal aortic dissection. While motion of the aorta in four dimensions can be traced with real-time imaging, displacement and rotation in quantitative terms remain unknown. The hypothesis was to show feasibility of quantification of three-dimensional aortic root motion from dynamic CT imaging.

Methods and results

Dynamic CT images of 40 patients for coronary assessment were acquired using a dynamic protocol. Scans were ECG-triggered and segmented in 10 time-stepped phases (0–90%) per cardiac cycle. With identification of the sinotubular junction (STJ), a patient-specific co-ordinate system was created with the *z*-axis (out-of-plane) parallel to longitudinal direction. The left and right coronary ostia were traced at each time-step to quantify downward motion in reference to the STJ plane, motion within the STJ plane (in-plane), and the degree of rotation. Enrolled individuals had an age of 65 ± 12, and 14 were male (35%). The out-of-plane motion was recorded with the largest displacement of 10.26 ± 2.20 and 8.67 ± 1.69 mm referenced by left and right coronary ostia, respectively. The mean downward movement of aortic root was 9.13 ± 1.86 mm. The largest in-plane motion was recorded at 9.17 ± 2.33 mm and 6.51 ± 1.75 mm referenced by left and right coronary ostia, respectively. The largest STJ in-plane motion was 7.37 ± 1.96 mm, and rotation of the aortic root was 11.8 ± 4.60°.

Conclusion

In vivo spatial and temporal displacement of the aortic root can be identified and quantified from multiphase ECG-gated contrast-enhanced CT images. Knowledge of normal 4D motion of the aortic root may help understand its biomechanical impact in patients with aortopathy and pre- and post-surgical or transcatheter aortic valve replacement.

* Corresponding author. E-mail: C.Nienaber@rbht.nhs.uk
† These authors contributed equally to this work.

Graphical Abstract

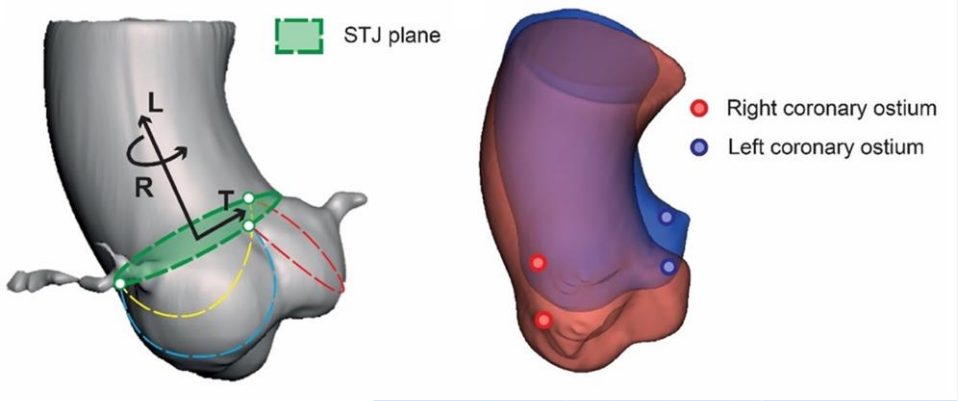

	Left coronary ostium	Right coronary ostium
Displacement (L) (mm)	10.26±2.20	8.67±1.69
Root rotation (degree)	11.8±4.60	

Keywords aortic root motion • root displacement • multiphase CT • dynamic imaging • aortic aneurysm • aortic dissection

Introduction

Aortic dissection is a rare but potentially life-threatening condition.[1] In addition to hypertension and aortic dilation,[2] the motion of the aortic root has also been suggested as conditional factor for dissection. During the cardiac cycle, the aortic annulus is exposed to ventricular traction in systole and relaxation in diastole.[3,4] Traction forces generated by the heart move the aortic annulus, causing motion transmitted to the ascending aorta. Aortic root motion has been shown to change in parallel with cardiovascular conditions such as left ventricular hypokinesis and aortic insufficiency. Since the supra-aortic vessels are relatively constrained compared with the ascending aorta, different aortic root motions can result in different levels of focal aortic wall stress, which has been proposed as a risk prediction index for aortic dissection.[5,6] Quantitative motion and stress parameters specific to certain tissue pathologies are not known yet.

Similar to motion, aortic wall stiffness is also thought to increase the risk of dissection.[7,8] Circumferential stress, largely related to blood pressure, is a reflection of aortic distensibility and pulse wave velocity. However, there are currently no diagnostic tests available to measure longitudinal wall stiffness of the ascending aorta. Three main dynamic mechanical factors may contribute to stress in the ascending aorta: systolic arterial blood pressure, blood flow characteristics, and motion of the aorta during cardiac cycle.[9] The latter is thought to significantly affect longitudinal stress in the ascending aorta.[10] However, clinical studies that examine the relationship between these parameters and aortic diameter, aortic wall stiffness, or the incidence of acute aortic syndromes are missing.

CT is the most widely and commonly used imaging modality for cardiovascular diagnosis.[11,12] Studies showed that ECG-gated CT angiogram can provide reliable measurements of ascending aorta by suppressing cardiac pulsation artefacts (i.e. aortic root motion).[12,13] With retrospective ECG gating, the entire cardiac cycle can be reconstructed, and reviewed with incorporation of dynamic information, the fourth dimension of CT imaging.[14]

The aim of this study was to quantify and describe the spatial motion of the aortic root during cardiac cycle (see Supplementary data online) in a cohort with no known cardiovascular disease.

Methods

Image selection

Dynamic CT images were retrieved from the picture and achieving system (PACS) of the Department of Radiology at Royal Brompton and Harefield Hospitals from January 2006 to December 2012. CTCA (CT cardiac angiogram) image data from 40 patients with no cardiovascular risk factors, no known coronary artery disease, or any aortic valve abnormality and normal ventricular function were chosen, if the following criteria were also fulfilled: (i) contrast-enhanced retrospective ECG-gated multidetector computed tomography (MDCT) of the heart; (ii) at least 10 cm of ascending aorta from aortic annulus scanned in the image set; (iii) 10 evenly time-stepped imaging acquisitions during one cardiac cycle; (iv) normal anatomy of aortic root and ascending aorta within the scanned volume; and (v) quality of image sufficient to identify commissures and coronary ostia. These CTCA scans were performed for clinical indications such as atypical chest pain to exclude coronary artery disease; no individual in this study cohort had a bicuspid aortic valve or any aortopathy. The study is in compliance with the Helsinki Declaration and has been ethically approved by Health Research Authority (IRAS project ID: 281535, REC reference: 20/PR/0835); patient's informed consent form was waived while retrospectively utilizing anonymised image data and demographics from electronic medical notes.

CTCA image acquisition

All CTCA scans were acquired on a 64-slice (Toshiba Aquilion, Otawara, Japan) MBCT scanner with retrospective ECG gating and 100 or 120 kVp. The patients received oral metoprolol (up to 100 mg) to reduce the heart rate < 60 bpm and sublingual glyceryl trinitrate (800 μg) before the procedure. The images were acquired at 0.5 mm collimation with variable tube rotation and pitch based on patient's heart rate. 60 to 80 mL of non-ionic, low-osmolar iodinated contrast agent (Iopromaide, Ultravist 370, Bayer Healthcare, Reading, UK) was administered intravenously using a dual-headed power injector. Scan image acquisition was commenced using bolus-tracking technique. The CTCA data were obtained at 0.5 mm collimation, spaced and reconstructed at 2.0 mm thickness at every 10% phase of cardiac cycle (from 0 to 90%) to be used for the final motion analysis. Conventionally, 30–40% and 70–80% of the R–R interval represent the systolic and diastolic phase, retrospectively.[15] The mean radiation dose was 13.1 mSv using a conversion factor of 0.014.

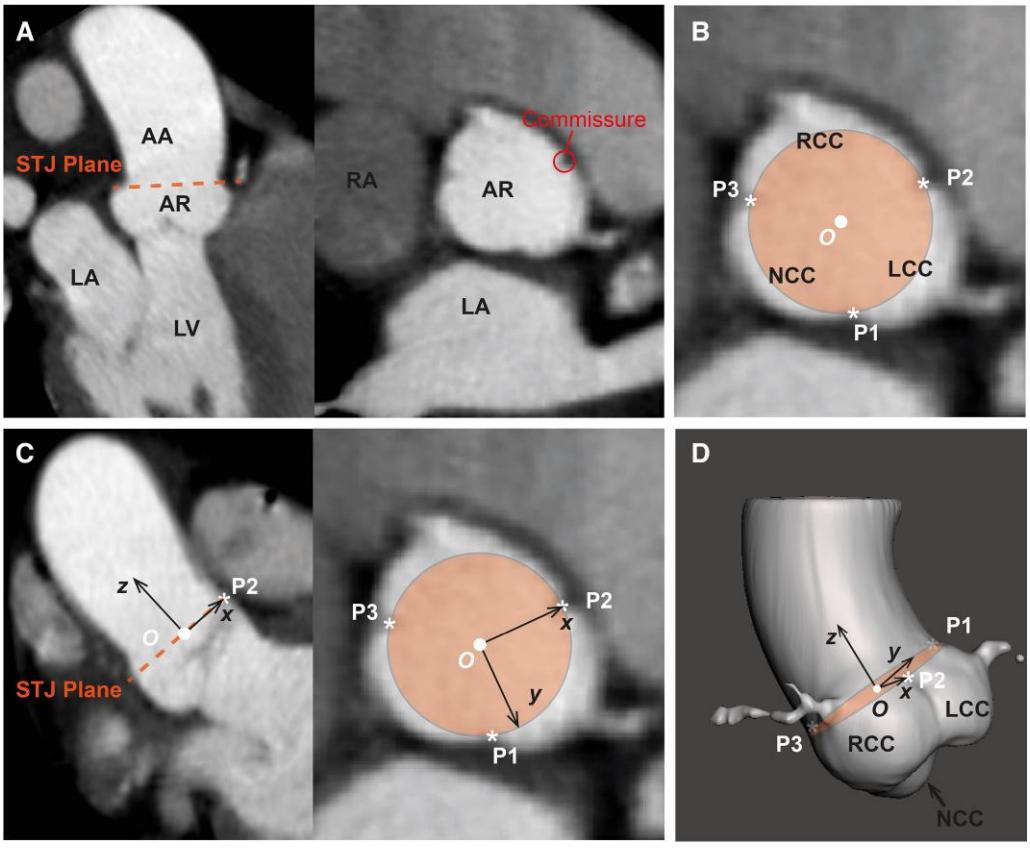

Figure 1 Definition of sinotubular junction (STJ) plane at TP_0 phase. (*A*) Anatomy of aortic root and heart. AA, ascending aorta; AR, aortic root; LA, left atrium; LV, left ventricle. (*B*) Anatomical landmarks to define the STJ plane (view perpendicular to the STJ plane). NCC, non-coronary cusp; RCC, right coronary cusp; LCC, left coronary cusp. Three commissures were marked as P1, P2, and P3, while *O* is the geometrical centre of three commissures. (*C*) Definition of the aortic root local co-ordinates. (*D*) View of the STJ plane and aortic root local co-ordinate in 3D.

Motion assessment

3D Slicer software (version 5.2.1, open source, BSD-style licence)[16] was employed for off-line image processing. Raw image data were anonymised and transferred to 3D Slicer (on an imaging processing PC) for sequencing and reconstruction. Zero per cent cardiac cycle phase (TP_0) at transverse plane was selected as reference phase for identifying the sinotubular junction (STJ) plane in each case (*Figure 1A*). Three commissures were marked by three landmark points (P1, P2, and P3) in the following order: non-coronary cusp (NCC) and left coronary cusp (LCC) (P1), LCC and right coronary cusp (RCC) (P2), then RCC-NCC (P3) to establish a patient-specific STJ plane in each case. The geometrical centre point of three commissures (*O*) was also calculated and defined as the origin of aortic root local co-ordinate (*Figure 1B*). Local normal direction of the STJ plane at point *O* is defined as *z*-direction of the local co-ordinate (*Figure 1C*), while the local *x*-direction is defined by the vector from point *O* to P2. The *y*-direction was defined by following the right-hand rule that is the cross product of unit vector in *z*-direction and *x*-direction (*Figure 1D*). In this scenario, the *y*-direction is not explicitly defined and without clinical meaning. Therefore, we choose to report the STJ in-plane displacement (d_{ip}) (refer to the displacement parallel to the STJ plane) rather than specific displacement into *x*-direction and *y*-direction.

Left and right coronary ostia were selected as anatomic markers (L_i for left coronary ostium and R_i for right coronary ostium, *i* represents the corresponding time-step phase number), while a mid-point (M_i) is defined as the geometrical centre of the left and right coronary ostia in the same phase to trace the spatial location and capture temporospatial aortic motion (*Figure 2*). Both the left and right coronary ostia were manually marked in each time-step phase (cardiac cycle 0–90%, TP_0 to TP_9) followed by mapping all markers (L_i, R_i, and M_i) onto the local aortic root co-ordinate system.

Total displacement of left and right coronary ostia as well as the mid-point within a cardiac cycle was calculated. Total displacement between time-step phases can be projected on the *z*-axis to calculate the out-of-plane displacement (d_{op}) (*Figure 3A*), and the displacement component projected on the STJ plane is defined as the in-plane displacement (d_{ip}) (*Figure 3B*). Thus, out-of-plane motion is defined as aortic root displacement along the perpendicular direction (z-direction) of the STJ plane (i.e. corresponding to aortic root downward motion), while in-plane motion is defined as aortic root displacement parallel to the STJ plane. Finally, the largest in-plane and out-of-plane displacements were calculated for each case.

For each frame, a vector from the left to the right coronary ostia is firstly defined, e.g. at the TP_0 frame the vector is defined as $\overrightarrow{L_0R_0}$. The maximum angle between all vectors ($\overrightarrow{L_0R_0}$ to $\overrightarrow{L_9R_9}$) is defined as the aortic root rotation angle (*r*) within a cardiac cycle; rotation was not decomposed into principal directions. Maximum aortic root rotation angle reported the maximum overall spatial rotation of aortic root within cardiac cycle landmarked by the left and right coronary ostia (*Figure 3C*). In an attempt to prove high inter-operator reproducibility, aortic motion assessment was performed strictly according to protocol and by two experienced specialists independently; each case was repeated three times to assess reproducibility in the attempt to minimize human error.

Statistical analysis

All statistical analyses were performed using SPSS® version 25 (IBM Corp. Armonk, NY, USA). Continuous variables were presented as mean and standard deviation or median and inter-quartile range; categorical variables were presented as frequencies and percentages. Pearson correlation was

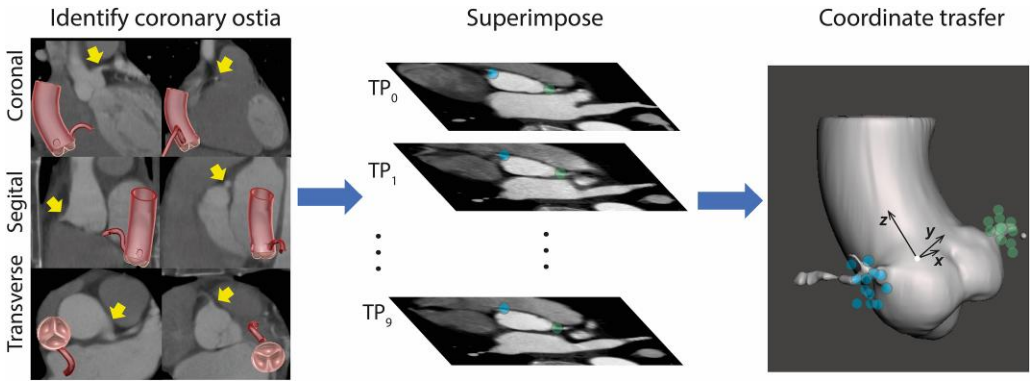

Figure 2 Summary of workflow.

employed to test each operator's reproducibility (intra-operator), while intraclass correlation coefficient (ICC) was employed to test data reliability from two independent aortic motion assessment operators (inter-operator). *P* values of <0.05 were considered statistically significant.

Results

The hypothesis to quantify aortic root motion was proved as aortic root motion was quantified in three dimensions that was then decomposed into out-of-plane displacement (d_{op}), in-plane displacement (d_{ip}), and rotation angle (r). A total of 40 eligible CT image datasets from 40 patients were retrieved and analysed.

Aortic root motion

The co-ordinates of commissures and coronary ostia were transferred to a local (patient-specific) aortic root co-ordinate system in each case. The geometrical centre of left and right coronary ostia was defined as mid-point (M_i) to represent the root and computed by the co-ordinates of left and right coronary ostia.

The out-of-plane motion (longitudinal) was recorded with the maximum displacement being 10.26 ± 2.20 mm and 8.67 ± 1.69 mm for the left and right coronary ostia, respectively. The out-of-plane displacement of the aortic root (marked by mid-point M) was 9.13 ± 1.86 mm. The STJ in-plane displacement was 9.17 ± 2.33 for the left coronary ostium and 6.51 ± 1.75 mm for the right coronary ostium. The aortic root in-plane displacement was 7.37 ± 1.96 mm (*Figure 4*) and the aortic root rotation angle (r) was 11.8 ± 4.60°.

Data reproducibility

Two experienced operators analysed and measured the images independently, but following the same processing protocol. Each operator repeated the motion measurement three times to allow assessment of inter- and intra-operator reproducibility. The results demonstrated strong reproducibility of displacement measurements with an *R*-value or linear correlation coefficient ranging from 0.885 to 0.947 ($P < 0.001$) and 0.883 to 0.959 ($P < 0.001$), for operators 1 and 2, respectively (*Table 1*). Similar reproducibility results were seen for rotation measurement with an *R*-value ranging from 0.835 to 0.912 ($P < 0.001$) and 0.876 to 0.932 ($P < 0.001$) for operators 1 and 2, respectively (*Figure 5*).

ICC was 0.96 for aortic root longitudinal displacement and 0.928 for aortic root rotation angle (*Table 2*), demonstrating excellent reproducibility between the two operators.

ICC results for the left and right coronary ostia in-plane displacement are also included in *Table 2*, which again showed good consistency between independent measurements by the two operators.

Discussion

Besides some quantitative observations from invasive contrast angiogram[4] and cardiovascular magnetic resonance (CMR),[3] little is known about quantitative assessment of aortic motion. This is the first report on quantitative measurements of aortic root motion in three dimensions in a cohort not affected by any aortopathy or aortic valve disease and provides a technical platform for studies in patient groups. Based on retrospective ECG-gated CT aortograms, the longitudinal (downward) motion of the aortic root was measured at 9.13 ± 1.86 mm and thus in the range to previously reported downward movement of the aortic annulus of 12.6 ± 3.6 mm (pre-PEARS) vs. 7.9 ± 2.9 mm (post-PEARS) using complex CMR.[3,17] Other had reported 7.1 ± 2.5 mm and 9.6 ± 3.4 mm by use of invasive aortography.[4,18] The feature of STJ in-plane motion of 7.37 ± 1.96 mm with an annulus rotation of 11.8 ± 4.60° has never been identified before and is reported for the first time. Thus, a relatively simple and pragmatic ECG-gated dynamic CT aortogram may offer a new view to the aortic root and provide reliable information aortic root motion in three dimensions.

Although dynamic changes in aortic diameter during the cardiac cycle have been described, quantitative analysis of systolic and diastolic changes at the level of the aortic root was not reported in previous human studies by MDCT.[15,19,20] Only experimental sonomicrometry studies in dogs[21] and finite element model analysis[22] had shown enlargement of the aortic root dimensions during systole compared with diastole. There is an ongoing discussion[23] about the mechanism by which the aortic root dilates prior to opening of the aortic valve, involving passive fluid dynamics or possibly even active processes that could be impeded in some pathologies.

Angiography and echocardiography are important imaging modalities for visualization of the aortic root but are difficult to provide quantitative information. With the advent of transcatheter aortic valve implantation procedures,[24–26] closed chest imaging becomes even more important, regarding value sizing, and accurate positioning of the prosthesis, to avoid coronary obstruction.[25,26] Currently used angiography is limited by its two-dimensional character.[15,19,20] Similar to advanced ultrasound imaging, MDCT can provide three-dimensional images with a high spatial resolution for detailed information on the anatomy of the aortic root and the relation of the annulus to coronary ostia.[15] The use of real-time 3D transoesophageal echocardiography (TOE) to guide cardiac interventions has increased over the last few years. Direct planimetry of the aortic annular area by 3D TOE volumetric imaging

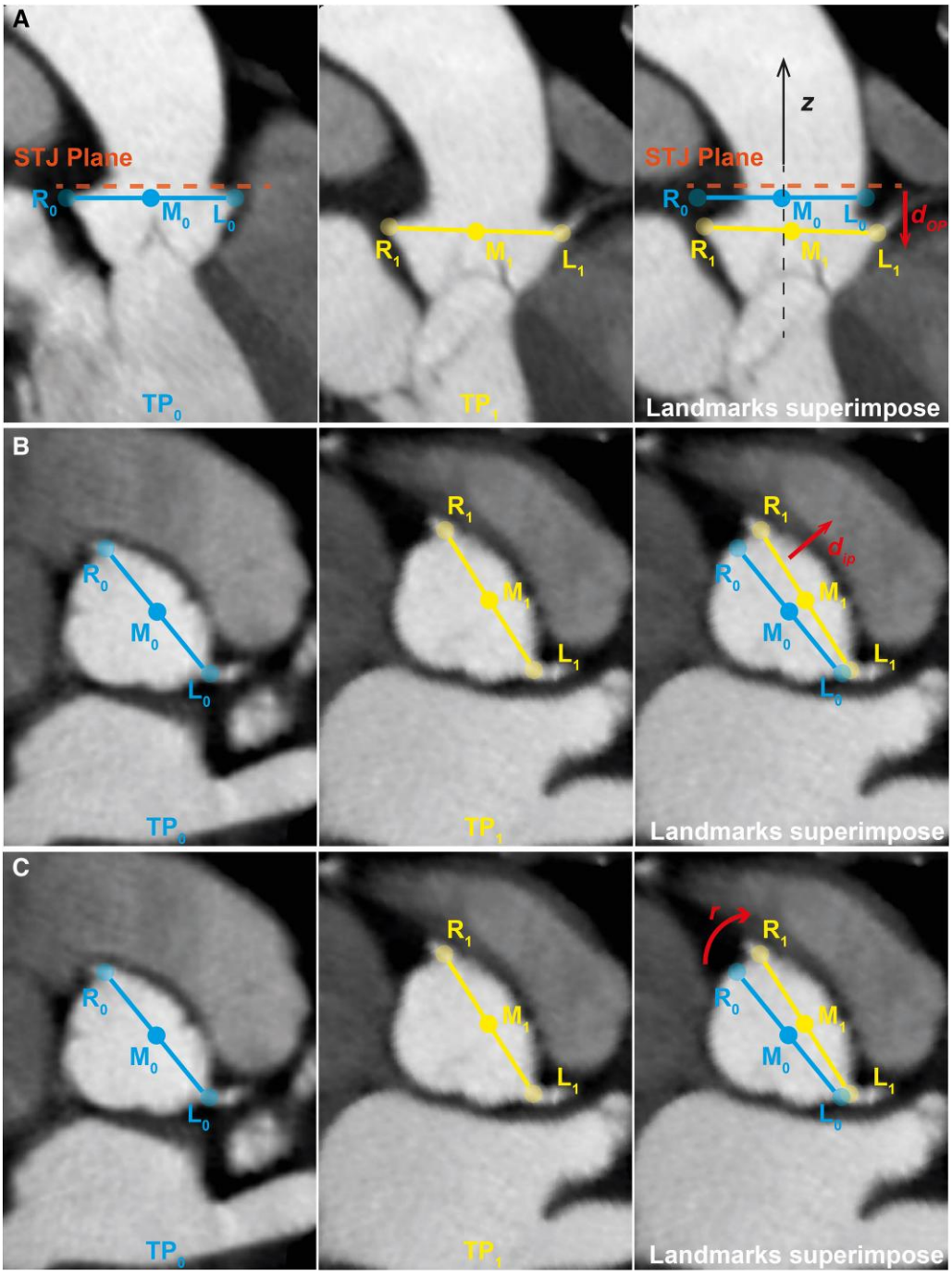

Figure 3 Definition of aortic root motion between time phases. (*A*) Out-of-plane displacement (d_{op}) is defined as the displacement in *z*-direction. (*B*) In-plane displacement (d_{ip}) is defined by projecting total displacement between time phases onto STJ plane. (*C*) aortic rotation angle (*r*) is defined as the angle between the left and right ostia connection lines at two consecutive time phases.

showed the best agreement with MDCT as a 'gold standard',[27] although still underestimating the MDCT planimetered areas by up to 9.6%, due to lower spatial resolution of 3D TOE volumetric imaging.[27]

Impact of aortic stiffness on aortic motion

The wall of aorta is a dynamic composite structure consisting of matrix macromolecules and vascular cells. Each component plays a role in determining the structure of aortic tissue, while disruption of any of these components can change the mechanical behaviour of the aortic wall.[28] Vascular calcification is a factor that is also associated with arterial stiffness, and a marker of cardiovascular diseases. Calcification occurs in the intimal and medial layers of arterial walls and causes decreased vascular elasticity[29,30] with aortic stiffness as a known predictor of cardiovascular mortality.[31]

Aortic motion and impact on wall stress

Aortic insufficiency admittedly leads to increased stroke volume as a compensatory mechanism, which is closely linked to an increase in aortic root displacement in its axial direction.[32] A relationship between stroke volume and increased aortic displacement in the frontal–dorsal direction has also been suggested based on 2D echocardiography.[33–35] Pulsations of the aorta in severe cases of aortic insufficiency are well known, and can even be transmitted to the patient's head (nodding or de Musset's sign). The augmenting impact of aortic insufficiency on aortic root displacement was already suggested 20 years ago[4] and confirmed by multivariate analysis.[32]

While the extent of aortic root motion and concomitant blood pressure and aortic wall stiffness determine aortic wall stress,[4] results of a wall stress analysis can be highly meaningful especially in a comparative sense. The 32% increase in longitudinal stress in the ascending aorta in patients with aortic insufficiency compared with normal value function goes along with a significant change in aortic root motion from 4.3 to 7.3 mm.[32] Even more detrimental effects are expected to be with larger displacement found in some patients.[32] Unfortunately, aortic root motion is commonly neglected in most biomechanical simulations of the ascending aorta, which may have impact on simulation results.[36]

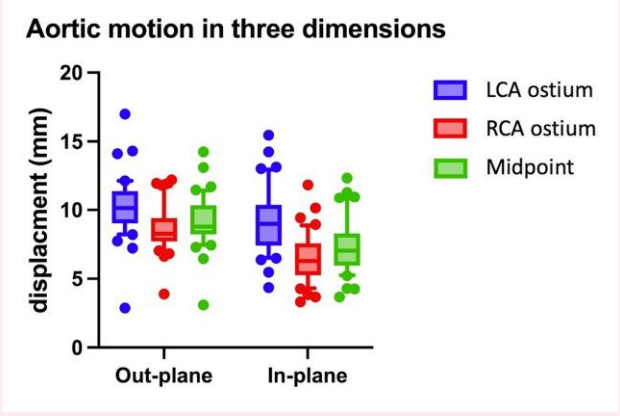

Figure 4 Aortic motion in three dimensions.

Concomitant aortic dilatation may also increase mechanical stress within the aorta. According to the fundamental Laplace law, under a pressure P, the circumferential and longitudinal stresses in a cylinder of a thickness *t* and radius R are PR/*t* and PR/2*t*, respectively.[37] With the wall thickness decreasing as the aorta dilates, both the circumferential and longitudinal stresses would increase and add to the risk of aortic dissection.

Impact of impaired 3D aortic motion on aortic pathologies

During a normal contraction cycle of the left ventricle, the movement of the aortic annulus towards the apex results in longitudinal stretch in the ascending aorta. Accordingly, the major systolic movement of the aortic root is downward; in-plane motion and clockwise axial twist were found to be not reluctant for longitudinal deformation.[5] Thus, aortic root displacement would be reduced in patients with the left ventricular systolic dysfunction lowing aortic wall stress.

In the future, non-invasive aortic root movement measures may identify patients at higher risk for progressive aortic enlargement and adverse clinical outcomes, potentially allowing for closer monitoring and more appropriate therapy in patients with cardiovascular diseases.[4,5,18,38] This could be important in populations with high risk of developing aortic dissection or aneurysmatic formation, including patients with bicuspid aortic valve and connective tissue disorders, especially Marfan's syndrome.

Unfortunately, the mere aortic diameter is not a good predictor of aortic dissection and additional parameters should be assessed for better risk prediction.[39] Impairment of elastic properties of the ascending aorta is a predictor of aortic complications in patients with bicuspid aortic valve.[40,41] Alterations of functionality often precede patho-anatomical changes in cardiovascular pathophysiology. Moreover, longitudinal strain on proximal aorta, but not circumferential strain and distensibility, was an independent predictor of aortic root growth rate in Marfan syndrome patients by using dynamic CMR.[42] The out-plane motion of the aortic root due to ventricular traction was suggested to contribute to aortic dissection by increasing its longitudinal stress; the largest aortic wall stress increase due to aortic root displacement was located ~20 mm above the STJ.[15] The implementation of dynamic CT imaging as part of a routine scan protocol would remarkably reduce invasiveness time and cost to provide information on stress and motion of the ascending aorta.

Table 1 Pearson correlation analyses on inter-operator reproducibility

			LCA ostium		RCA ostium		Mid-point		Rotation
			In-plane	Out-plane	In-plane	Out-plane	In-plane	Out-plane	
Operator 1	1st vs. 2nd attempt	r	0.885	0.922	0.945	0.920	0.945	0.893	0.912
		P	<0.001	<0.001	<0.001	<0.001	<0.001	<0.001	<0.001
	1st vs. 3rd attempt	r	0.903	0.893	0.947	0.912	0.923	0.936	0.835
		P	<0.001	<0.001	<0.001	<0.001	<0.001	<0.001	<0.001
	2nd vs. 3rd attempt	r	0.930	0.925	0.953	0.909	0.935	0.923	0.907
		P	<0.001	<0.001	<0.001	<0.001	<0.001	<0.001	<0.001
Operator 2	1st vs. 2nd attempt	r	0.938	0.951	0.927	0.883	0.959	0.943	0.932
		P	<0.001	<0.001	<0.001	<0.001	<0.001	<0.001	<0.001
	1st vs. 3rd attempt	r	0.915	0.936	0.903	0.909	0.931	0.921	0.903
		P	<0.001	<0.001	<0.001	<0.001	<0.001	<0.001	<0.001
	2nd vs. 3rd attempt	r	0.948	0.937	0.924	0.932	0.928	0.931	0.876
		P	<0.001	<0.001	<0.001	<0.001	<0.001	<0.001	<0.001

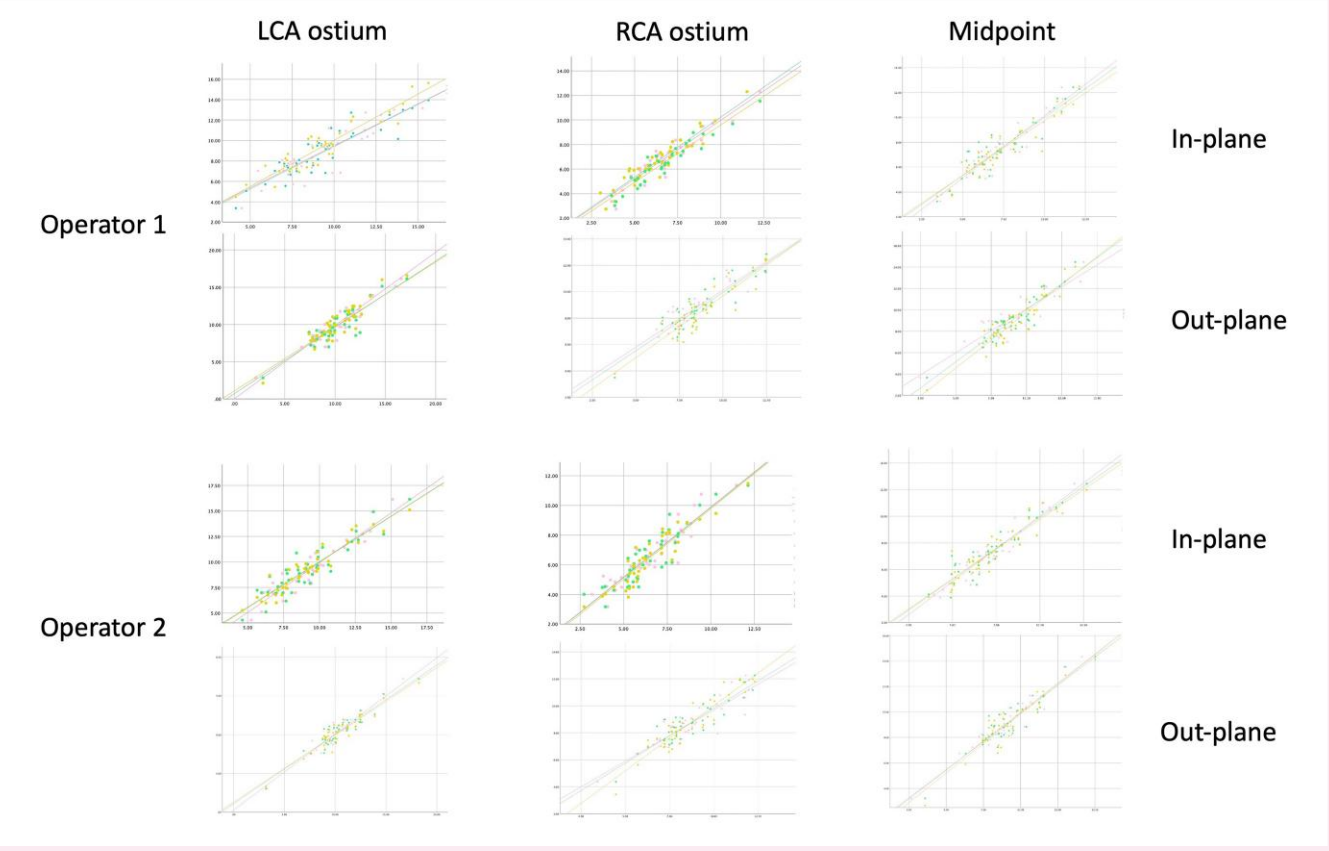

Figure 5 Pearson correlation analyses on inter-operator reproducibility.

Table 2 Intraclass correlation analyses on intra-operator reproducibility

	LCA ostium		RCA ostium		Mid-point		rotation
	In-plane	Out-plane	In-plane	Out-plane	In-plane	Out-plane	
ICC	0.930	0.916	0.615	0.942	0.952	0.960	0.928
P	<0.001	<0.001	<0.001	<0.001	<0.001	<0.001	<0.001

Limitations

Natural 4D motion was identified and measured by manual tracing potentially involving human error or bias. To minimize human error, inter- and intra-person reliability was tested and showed good data reproducibility. As artificial intelligence-based image recognition techniques are evolving, more precise and accurate motion assessment methods will eventually even improve the quality of motion quantification.

Our observations were made in a relatively small cohort (40 patients) from two cardiovascular centres, but robust methodology was used to quantify aortic root motion with a retrospective ECG-gate CT angiogram. In this study, we only demonstrate the potential to perform 3D quantitative motion analysis of the aortic root, but larger prospective studies wound be required to assess the relationship of aortic root motion to the outcomes in terms of aortic dilatation and dissection.

Compared with CMR, CTA can provide geometry information with better spatial resolution (smaller slice thickness) of anatomical details after contrast enhancement, allowing quantification of 3D motion, especially rotation of the aortic root. Although CTA acquired during the whole cardiac cycle will increase radiation dose slightly, comprehensive scrutiny safety analysis deemed the imaging protocol to be safe with a 0.048% increased risk of cancer burden; with the most modern CT scanner, the extra radiation dose would be even lower.

Conclusion

The *in vivo* spatial and temporal displacement of the aortic root can be identified and quantified from multiphase ECG-gated contrast-enhanced dynamic CT images. Knowledge of normal 3D motion of the aortic root may help understand the biomechanical impact of impaired 3D motion in normal individuals and patients with any aortopathy.

Supplementary data

Supplementary data are available at *European Heart Journal – Imaging Methods and Practice* online.

Conflict of interest: None declared.

Funding

The authors acknowledge the Lee Family Scholarship for the support of X.Y.

Consent: Patient's informed consent form was waived while retrospectively utilising anonymised image data and demographics from electronic medical notes.

Data availability

The data underlying this article will be shared on reasonable request to the corresponding author; data are essentially dynamic CT image files subjected to semi-automated software based analysis for motion.

Lead author biography

Professor Nienaber is a consultant cardiologist at Royal Brompton Hospital, with his research and clinical activities focused on the diagnosis and non-surgical treatment of acute and chronic aortic pathologies, such as aneurysms and aortic dissection. His role sees him consult with patients who have aortic conditions, and their families, to help them understand their disease better and provide the best treatment option. He is the co-founder of IRAD (International Registry of Aortic Dissection), which operates as a global network for acute aortic conditions. Through this, he has pioneered new endovascular techniques to treat aortic dissection and initiated and participated in guideline-changing trials. His research also encompasses modern interventional approaches to structural heart disease, including: transcatheter aortic valve implantation (TAVI)thoracic endovascular aortic repair (TEVAR)left-atrial appendage occlusion patent foramen ovaleatrial septal defect II-occlusion nonsurgical management of aortic coarctation and malformations.

Ethical approval

This study is in compliance with the Helsinki Declaration and has been ethically approved by Health Research Authority (IRAS project ID: 281535, REC reference: 20/PR/0835).

References

1. Nienaber CA, Clough RE, Sakalihasan N, Suzuki T, Gibbs R, Mussa F *et al.* Aortic dissection. *Nat Rev Dis Primers* 2016;**2**:16071.
2. Erbel R, Aboyans V, Boileau C, Bossone E, Bartolomeo RD, Eggebrecht H *et al.* 2014 ESC guidelines on the diagnosis and treatment of aortic diseases: document covering acute and chronic aortic diseases of the thoracic and abdominal aorta of the adult. The Task Force for the Diagnosis and Treatment of Aortic Diseases of the European Society of Cardiology (ESC). *Eur Heart J* 2014;**35**:2873–926.
3. Singh SD, Xu XY, Pepper JR, Izgi C, Treasure T, Mohiaddin RH. Effects of aortic root motion on wall stress in the Marfan aorta before and after personalised aortic root support (PEARS) surgery. *J Biomech* 2016;**49**:2076–84.
4. Beller CJ, Labrosse MR, Thubrikar MJ, Robicsek F. Role of aortic root motion in the pathogenesis of aortic dissection. *Circulation* 2004;**109**:763–9.
5. Wei W, Evin M, Rapacchi S, Kober F, Bernard M, Jacquier A *et al.* Investigating heartbeat-related in-plane motion and stress levels induced at the aortic root. *Biomed Eng Online* 2019;**18**:19.
6. Plonek T, Zak M, Burzynska K, Rylski B, Gozdzik A, Kustrzycki W *et al.* The combined impact of mechanical factors on the wall stress of the human ascending aorta—a finite elements study. *BMC Cardiovasc Disord* 2017;**17**:297.
7. Vitarelli A, Conde Y, Cimino E, D'Angeli I, D'Orazio S, Stellato S *et al.* Aortic wall mechanics in the Marfan syndrome assessed by transesophageal tissue Doppler echocardiography. *Am J Cardiol* 2006;**97**:571–7.
8. Rajzer M, Wojciechowska W, Kameczura T, Olszanecka A, Fedak D, Terlecki M *et al.* The effect of antihypertensive treatment on arterial stiffness and serum concentration of selected matrix metalloproteinases. *Arch Med Sci* 2017;**13**:760–70.
9. Martufi G, Forneris A, Appoo JJ, Di Martino ES. Is there a role for biomechanical engineering in helping to elucidate the risk profile of the thoracic aorta? *Ann Thorac Surg* 2016;**101**:390–8.
10. Plonek T, Rylski B, Dumanski A, Siedlaczek P, Kustrzycki W. Biomechanical analysis of wrapping of the moderately dilated ascending aorta. *J Cardiothorac Surg* 2015;**10**:106.
11. Vilacosta I, San Roman JA, di Bartolomeo R, Eagle K, Estrera AL, Ferrera C *et al.* Acute aortic syndrome revisited: JACC state-of-the-art review. *J Am Coll Cardiol* 2021;**78**:2106–25.
12. Hachulla AL, Ronot M, Noble S, Becker CD, Montet X, Vallee JP. ECG-triggered high-pitch CT for simultaneous assessment of the aorta and coronary arteries. *J Cardiovasc Comput Tomogr* 2016;**10**:407–13.
13. Kozerke S, Scheidegger MB, Pedersen EM, Boesiger P. Heart motion adapted cine phase-contrast flow measurements through the aortic valve. *Magn Reson Med* 1999;**42**:970–8.
14. Schernthaner RE, Stadler A, Beitzke D, Homolka P, Weber M, Lammer J *et al.* Dose modulated retrospective ECG-gated versus non-gated 64-row CT angiography of the aorta at the same radiation dose: comparison of motion artifacts, diagnostic confidence and signal-to-noise-ratios. *Eur J Radiol* 2012;**81**:e585-90.
15. Tops LF, Wood DA, Delgado V, Schuijf JD, Mayo JR, Pasupati S *et al.* Noninvasive evaluation of the aortic root with multislice computed tomography implications for transcatheter aortic valve replacement. *JACC Cardiovasc Imaging* 2008;**1**:321–30.
16. Fedorov A, Beichel R, Kalpathy-Cramer J, Finet J, Fillion-Robin JC, Pujol S *et al.* 3D slicer as an image computing platform for the quantitative imaging network. *Magn Reson Imaging* 2012;**30**:1323–41.
17. Izgi C, Nyktari E, Alpendurada F, Bruengger AS, Pepper J, Treasure T *et al.* Effect of personalized external aortic root support on aortic root motion and distension in Marfan syndrome patients. *Int J Cardiol* 2015;**197**:154–60.
18. Plonek T, Rylski B, Nawrocki P, Beyersdorf F, Jasinski M, Kuliczkowski W. Systolic stretching of the ascending aorta. *Arch Med Sci* 2021;**17**:25–30.
19. Wood DA, Tops LF, Mayo JR, Pasupati S, Schalij MJ, Humphries K *et al.* Role of multislice computed tomography in transcatheter aortic valve replacement. *Am J Cardiol* 2009;**103**:1295–301.
20. Kazui T, Izumoto H, Yoshioka K, Kawazoe K. Dynamic morphologic changes in the normal aortic annulus during systole and diastole. *J Heart Valve Dis* 2006;**15**:617–21.
21. Thubrikar M, Harry R, Nolan SP. Normal aortic valve function in dogs. *Am J Cardiol* 1977;**40**:563–8.
22. Gnyaneshwar R, Kumar RK, Balakrishnan KR. Dynamic analysis of the aortic valve using a finite element model. *Ann Thorac Surg* 2002;**73**:1122–9.
23. Vesely I. Aortic root dilation prior to valve opening explained by passive hemodynamics. *J Heart Valve Dis* 2000;**9**:16–20.
24. Cribier A, Eltchaninoff H, Tron C, Bauer F, Agatiello C, Nercolini D *et al.* Treatment of calcific aortic stenosis with the percutaneous heart valve: mid-term follow-up from the initial feasibility studies: the French experience. *J Am Coll Cardiol* 2006;**47**:1214–23.
25. Webb JG, Chandavimol M, Thompson CR, Ricci DR, Carere RG, Munt BI *et al.* Percutaneous aortic valve implantation retrograde from the femoral artery. *Circulation* 2006;**113**:842–50.
26. Grube E, Laborde JC, Gerckens U, Felderhoff T, Sauren B, Buellesfeld L *et al.* Percutaneous implantation of the CoreValve self-expanding valve prosthesis in high-risk patients with aortic valve disease: the Siegburg first-in-man study. *Circulation* 2006;**114**:1616–24.
27. Ng AC, Delgado V, van der Kley F, Shanks M, van de Veire NR, Bertini M *et al.* Comparison of aortic root dimensions and geometries before and after transcatheter aortic valve implantation by 2- and 3-dimensional transesophageal echocardiography and multislice computed tomography. *Circ Cardiovasc Imaging* 2010;**3**:94–102.
28. Emmott A, Garcia J, Chung J, Lachapelle K, El-Hamamsy I, Mongrain R *et al.* Biomechanics of the ascending thoracic aorta: a clinical perspective on engineering data. *Can J Cardiol* 2016;**32**:35–47.
29. Lacolley P, Regnault V, Segers P, Laurent S. Vascular smooth muscle cells and arterial stiffening: relevance in development, aging, and disease. *Physiol Rev* 2017;**97**:1555–617.
30. Vlachopoulos C, Aznaouridis K, Stefanadis C. Prediction of cardiovascular events and all-cause mortality with arterial stiffness: a systematic review and meta-analysis. *J Am Coll Cardiol* 2010;**55**:1318–27.
31. Collette M, Humeau A, Chevalier C, Hamel JF, Leftheriotis G. Assessment of aortic stiffness by local and regional methods. *Hypertens Res* 2011;**34**:578–83.
32. Beller CJ, Labrosse MR, Thubrikar MJ, Szabo G, Robicsek F, Hagl S. Increased aortic wall stress in aortic insufficiency: clinical data and computer model. *Eur J Cardiothorac Sur* 2005;**27**:270–5.
33. Duvernoy O, Coulden R, Ytterberg C. Aortic motion: a potential pitfall in CT imaging of dissection in the ascending aorta. *J Comput Assist Tomogr* 1995;**19**:569–72.
34. Pratt RC, Parisi AF, Harrington JJ, Sasahara AA. The influence of left ventricular stroke volume on aortic root motion: an echocardiographic study. *Circulation* 1976;**53**:947–53.
35. Keltai M, Lengyel M, Tonelli M, Gabor G. Aortic root motion for the assessment of left ventricular function in acute myocardial infarction. *Acta Cardiol* 1979;**34**:51–6.

36. Wang Z, Flores N, Lum M, Wisneski AD, Xuan Y, Inman J *et al.* Wall stress analyses in patients with ≥5 cm versus <5 cm ascending thoracic aortic aneurysm. *J Thorac Cardiovasc Surg* 2021;**162**:1452–9.
37. Thubrikar MJ, Agali P, Robicsek F. Wall stress as a possible mechanism for the development of transverse intimal tears in aortic dissections. *J Med Eng Technol* 1999;**23**: 127–34.
38. Tierney ES S, Levine JC, Sleeper LA, Roman MJ, Bradley TJ, Colan SD *et al.* Influence of aortic stiffness on aortic-root growth rate and outcome in patients with the Marfan syndrome. *Am J Cardiol* 2018;**121**:1094–101.
39. Pape LA, Tsai TT, Isselbacher EM, Oh JK, O'Gara P T, Evangelista A *et al.* Aortic diameter ≥ 5.5 cm is not a good predictor of type A aortic dissection: observations from the International Registry of Acute Aortic Dissection (IRAD). *Circulation* 2007;**116**: 1120–7.
40. Longobardo L, Carerj ML, Pizzino G, Bitto A, Piccione MC, Zucco M *et al.* Impairment of elastic properties of the aorta in bicuspid aortic valve: relationship between biomolecular and aortic strain patterns. *Eur Heart J Cardiovasc Imaging* 2018;**19**:879–87.
41. Longobardo L, Carerj S, Bitto A, Cusma-Piccione M, Carerj ML, Calabro MP *et al.* Bicuspid aortic valve and aortopathy: novel prognostic predictors for the identification of high-risk patients. *Eur Heart J Cardiovasc Imaging* 2021;**22**:808–16.
42. Guala A, Teixido-Tura G, Rodriguez-Palomares J, Ruiz-Munoz A, Dux-Santoy L, Villalva N *et al.* Proximal aorta longitudinal strain predicts aortic root dilation rate and aortic events in Marfan syndrome. *Eur Heart J* 2019;**40**:2047–55.